Towards chemotactic supramolecular nanoparticles: From autonomous surface motion following specific chemical gradients to multivalency-controlled disassembly

Chiara Lionello,[†,a] Andrea Gardin,[†,a] Annalisa Cardellini,[a] Davide Bochicchio,[b,c] Manisha Shivrayan,[d] Ann Fernandez,[d] S. Thayumanavan[d] & Giovanni M. Pavan[a,b,]*

[a] Politecnico di Torino, Department of Applied Science and Technology, Corso Duca degli Abruzzi 24, Torino, 10129, Torino, Italy

giovanni.pavan@polito.it

[b] Department of Innovative Technologies, University of Applied Sciences and Arts of Southern Switzerland, Polo Universitario Lugano, Campus Est, Via la Santa 1, 6962 Lugano-Viganello, Switzerland

[c] Department of Physics, Universit_a degli studi di Genova, Via Dodecaneso 33, 16100 Genova, Italy

[d] Department of Chemistry, Center for Bioactive Delivery at the Institute for Applied Life Sciences, University of Massachusetts, Amherst, Massachusetts 01003, United States

[†] These authors contributed equally to the work

KEYWORDS chemotaxis, nanoparticles, stimuli-responsive, self-assembly, coarse-graining, molecular simulation, autonomous motion, surface binding

ABSTRACT. Nature designs chemotactic supramolecular structures that can selectively bind specific groups present on surfaces, autonomously scan them moving along density gradients, and react once a critical concentration is encountered. While such properties are key in many biological functions, these also offer inspirations for designing artificial systems capable of similar bioinspired autonomous behaviors. One approach is to use soft molecular units that self-assemble in aqueous solution generating nanoparticles (NPs) that display specific chemical groups on their surface, enabling for multivalent interactions with complementarily functionalized surfaces. However, a first challenge is to explore the behavior of these assemblies at sufficiently high-resolution to gain insights on the molecular factors controlling their behaviors. Here we show that, coupling coarse-grained molecular models and advanced simulation approaches, it is possible to study the (autonomous or driven) motion of self-assembled NPs on a receptor-grafted surface at submolecular resolution. As an example, we focus on self-assembled NPs composed of facially amphiphilic oligomers. We observe how tuning the multivalent interactions between the NP and the surface allows to control NP binding, its diffusion along chemical surface gradients, and ultimately, the NP reactivity at determined surface group densities. *In silico* experiments provide physical-chemical insights on key molecular features in the self-assembling units which determine the dynamic behavior and fate of the NPs on the surface: from adhesion, to diffusion, and disassembly. This offers a privileged point of view into the chemotactic properties of supramolecular assemblies, improving our knowledge on how to design new types of materials with bioinspired autonomous behaviors.

Nature offers numerous examples of supramolecular structures with fascinating dynamical chemotactic properties and stimuli-responsive behaviors[1,2]. Cells, for example, can sense the density and distribution of extracellular matrix (ECM) molecules by means of surface proteins (integrins) and complexes.[1,2] Such spatial sensing, based on the selective recognition/binding of ligands, controls and regulates the cellular activity in a variety of contexts.[3–5] A specific example is offered by leukocytes, which recognize and react to surface markers indicative of an infection[1,5–9]. In particular, leukocytes bind to the surfaces of blood capillaries, roll and scan surface markers, slow down, stop and release inflammatory signals. Such binding, rolling and reacting capabilities are controlled by a complex interplay between protein-protein and protein-carbohydrate interactions at the inter-face.[10–16] While mimicking the complexity and autonomous fidelity of the immune system is a daunting challenge, imparting similar autonomous functionalities to synthetic materials (Figure 1a) would be a breakthrough in many fields, from biomedicine, to sensing, and adaptive materials. However, addressing this challenge requires gaining fundamental insights on the molecular factors controlling the selective non-covalent interactions and the complex interplay (and competition) between them at the interface. Notable examples of synthetic supramolecular structures, such as fibers, vesicles, or tubes have demonstrated to have excellent stimuli responsive properties while autonomously moving.[6–10,11,12] Also responsive nanoparticles (NPs) have shown surface binding capability combined with tailored releasing of encapsulated guests.[13–17] In order to predict and engineering the selective binding on surfaces both monovalent and multivalent affinity are exploited. To cite just a few examples, Liao *et al.* studied the correlation be-tween monovalent labelling schemes on a gold NP and its diffusion rate on supported lipid bilayer membranes,[18] while Overseem and coworkers investigated multivalent binding profiles of influenza virus on surfaces with receptor density gradients.[19] However, despite notable advances

in surface modification and control are emerging thanks to cutting-edge techniques[20], technical experimental limitations still prevent the rational design of chemotactic functional materials. First, tracking and observing the movement of soft, tiny NPs on surfaces at sufficiently small spatiotemporal scales is a hard challenge.[21,22] Second, gaining insights on the molecular factors and processes that govern the NP chemotactic responsive behavior is even more complex, as it requires observing these materials in action at a submolecular resolution.

Molecular models and computer simulations are fundamental to reach this goal. Recent simulations using minimalistic coarse-grained (CG) models allowed to study the adhesion and dynamics of nanoparticles/cells (represented as single spheres) onto ligand-functionalized surfaces.[23–26] These models permitted to relate the number of interactions between the spherical nanoparticle (NP) and the surface receptors to the surface adhesion[26,27]. Similar CG models also allowed to simulate and monitor the rolling of a deformable (soft) spherical cell model on surfaces under the presence of an external flow.[24] Recently, Debets et al. simulated and analyzed the diffusion profile of a NP (modeled as a single sphere) on a fully cross-linked membrane CG model. Specifically, variations of surface receptor density and multivalent interactions between NP and gel-like membrane were observed to have remarkable effects on the diffusivity of the NP, eventually inducing NP trapping in high-density regions.[27] Although these interesting studies allowed to provide evidences of autonomous NP movement on surfaces, finer-level molecular models are needed in the perspective of designing supramolecular assemblies (e.g. self-assembled NPs) which can selectively bind surfaces, autonomously scan them moving along chemical surface gradients, and trigger controlled dynamic responses (*e.g.*, NP binding, rolling, disassembly, and release of encapsulated guests). This requires (i) to model the NP as an assembly of monomers (as the supramolecular structure of the NP must be explicitly taken into account in order to explore

NP destabilization and disassembly) and (ii) to keep the resolution in the molecular models high enough to obtain chemically relevant insight into the molecular factors that control the behavior/fate of the NP on the surface. For example, it has been shown that ~5 Å resolution CG models, coupled to advanced molecular simulations and analysis, allows to obtain precious links between the structure of monomers and the structure, dynamics and dynamic properties of the supramolecular assemblies that these generate.[13,28–31] *In silico* simulations provided a privileged point of view into the response of supramolecular polymeric materials to different biorelevant stimuli, such as *e.g.*, changes in temperature, salts, solvents, light, etc.[13,32,33] All atom molecular dynamics (AA-MD) simulations of protein-responsive assemblies allowed to compare the self-assembly stability of NPs composed of soft amphiphilic oligomers bearing biotin ligands (monomer-monomer interactions) with specific and non-specific interactions with complementary extravidin. In particular, it was demonstrated how specific binding events with the complementary protein was capable of destabilizing the assembled NPs[13]. However, it is worth noting that fascinating bioinspired properties such as chemotaxis have an intrinsically dynamic character. This opens the challenge of studying the dynamic behavior of chemotactic assemblies at high (submolecular) resolution, in search of molecularly relevant information on how to control them.

Here we designed a reverse multiscale modeling approach to reach this goal. Starting from minimalistic CG models of supramolecular NPs which can selectively bind groups present on surfaces, we use classical and advanced simulation approaches to study their dynamic chemotactic behavior. Focusing on realistic example of supramolecular assemblies, we then increase the resolution of our models and investigate viable molecular ways to control the autonomous behavior of the responsive NPs on the surface. *In silico* experiments finally show us how to control the chemotactic properties and the dynamic disassembly of the supramolecular NPs. This multiscale

approach offers a flexible platform toward the rational design of assembled structures with programmable autonomous chemotactic properties.

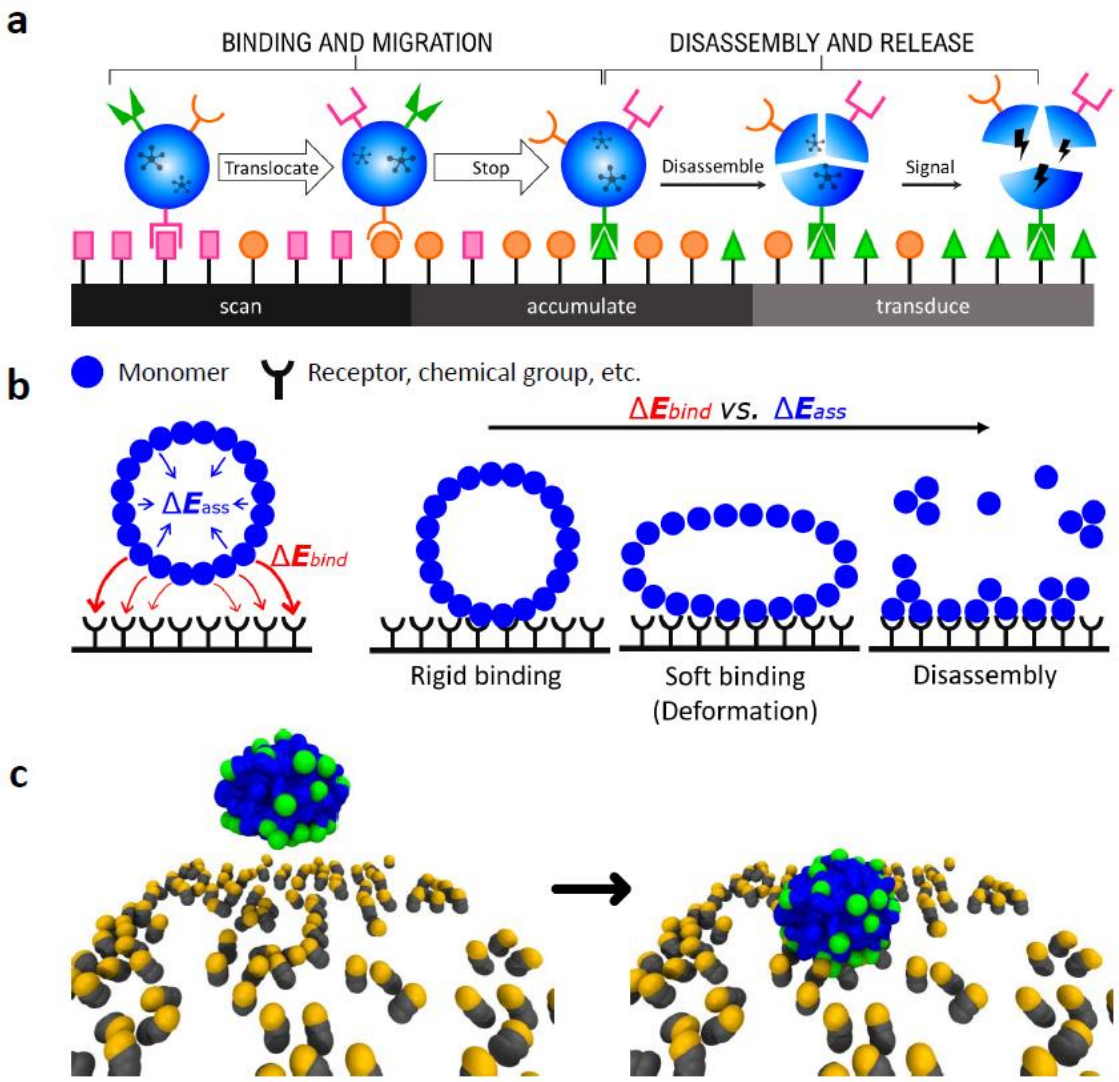

Figure 1. Multivalent adhesion and chemotaxis in natural and synthetic assemblies. a) Cells (*e.g.*, leukocytes) can bind and autonomously roll/translocate on surfaces, scanning them and releasing (inflammatory) signals in the presence of high-densities of surface markers indicative of, *e.g.*, an infection. b) Minimalistic CG model of a self-assembled NP. When establishing a multivalent binding with a complementary functionalized surface, the NP's fate depends on the competition between the monomers-receptors interactions (ΔE_{bind}: in red) and the monomer-monomer self-assembly energy (ΔE_{ass}: preserving the assembled structure, in blue). Whether the ΔE_{ass} globally prevail, compete with the ΔE_{bind}, or is dominated by the latter, would result in a rigid, soft adhesion, or even in the disassembly of the NP. c) Example molecular model of a supramolecular NP (monomers colored in blue and green) before (left) and after adhesion (right) on a ligand-coated surface (ligands in gray, active binding groups in orange).

RESULTS AND DISCUSSION

Chemotaxis of a supramolecular nanoparticle. Tracking and monitoring the dynamic behavior of soft assemblies on receptor-functionalized surfaces is crucial to understand how to design new types of artificial chemotactic NPs. We start from considering a supramolecular NP composed of self-assembling units (monomers) possessing ligands, or chemical groups, capable of establishing specific interactions with a complementary functionalized surface (Figure 1b). The fate of such a NP upon surface adhesion will essentially depend on the competition between the self-interactions of monomers in the assembly (ΔE_{ass}) and the multivalent interactions (ΔE_{bind}) with the surface. While the ΔE_{ass} governs the stability of the assembly, the ΔE_{bind} relates to the strength of specific interactions be-tween the groups present on the monomers (*e.g.*, ligands, chemical groups, etc.) and the complementary ones on the surface (*e.g.*, receptors, complementary chemical groups). In fact, self-assembled polymeric NPs and micelles are far from behaving as rigid spheres. These are soft entities which may deform upon surface contact in the attempt of maximizing the interactions with the surface receptors by enlarging the contact area (Figure 1b). The interplay between ΔE_{bind} and ΔE_{ass} may produce different scenarios upon NP binding to the surface: (i) a rigid adhesion (for $\Delta E_{ass} >> \Delta E_{bind}$: NP-surface binding has a negligible effect on the NP integrity), (ii) a soft adhesion accompanied by NP deformation (for $\Delta E_{ass} \sim \Delta E_{bind}$), or (iii) a potential destabilization and disassembly of the NP (for $\Delta E_{ass} << \Delta E_{bind}$). To challenge this simplistic scheme, herein we used coarse-grained (CG) molecular models (*e.g.*, Figure 1c).

We started developing a minimalistic CG model for a supramolecular NP composed of 1925 monomer units, each represented as a single CG particle (molecular resolution). To model the surface, we used a one-CG bead per-receptor group description, and we designed the surface in

such a way to obtain two different (low and high) density areas on the surface. In the lower density region, the groups density is 1/64 than in the higher density region (Figure 2). The ΔE_{bind} and ΔE_{ass} interaction energies are modeled via Lennard-Jones (LJ) potentials (defined by LJ variables σ and ε). Such a CG minimalistic model is approximated, and aims at providing general scope, and qualitative insights. The interactions between the CG particles in the model have been initially adjusted to obtain a $\Delta E_{ass}/\Delta E_{bind}$ ratio of ~¼ (similar to that recently estimated for self-assembling oligomers containing a biotin ligand able to specifically bind avidin).[13]

In this minimalistic model the monomer-monomer affinity, ΔE_{ass}, is described by a 12-6 LJ potential using σ = 0.47 nm and ε = 10 kJ mol^{-1}, while the monomer-receptor interaction, ΔE_{bind}, is described by a 12-6 LJ potential using σ = 0.35 nm and ε = 40 kJ mol^{-1} parameters. On the entire surface, we added a weakly attractive potential (2.0 kJ mol^{-1}, 20 times weaker than the specific interactions), which mimics weak non-specific interactions between the NP and the surface in receptor-free surface regions. CG-MD simulations using such a simplified model show that the NP, even initially placed in proximity of the surface in the low receptor density region, tends to rapidly bind the surface, impeding the movement. Despite the rescaling of the specific ΔE_{bind} monomer-receptor interactions (set to 40 kJ mol^{-1} in this CG model, while specific ligand-receptor interaction may be stronger – see the case of, for example, biotin-avidin binding, reaching ~80 kJ mol^{-1})[13], the characteristic timescales to escape the first NP-surface interactions exceed the typical timescales accessible by classical CG-MD simulations, which for this reason were found ineffective to study the dynamics of the system. Proven useful to study rare events in other complex supramolecular systems[11,34], we turned to an enhanced sampling approach, using metadynamics (MetaD) simulations to activate and explore the mechanism of motion of the NP on the surface. Depositing an energy bias on the *x* and *y* coordinates of the NP's center of mass, CG-MetaD

simulations allowed us to monitor the movement of the NP the surface. It is worth noting that such MetaD scheme biases only the position of the NP on the *xy* plane, while no constraint along *z* direction is imposed to the NP during the simulation. In this way, the biased simulation setup activates a random change of NP position on the *xy* plane, favoring a random walk on the surface where the NP can either slide, translate, roll or in principle even bounce on/off the surface.

These CG-MetaD simulations showed the NP moving in time from low to high density receptor regions on the surface, rolling in denser receptor regions and diffusing/sliding in the absence of receptors. No NP jumping was observed, highlighting how weak non-specific interactions (in receptor-free regions) are enough to retain the NP in proximity of the surface. Although these CG-MetaD simulations have a purely explorative purpose (prohibitive convergence), these simulations provide a qualitative indication on the diffusion pathways of the NP on a receptor-functionalized surface. The observed diffusion of the NP on the surface is a combination of (i) the Brownian motion of the NP in a thermalized regime, and (ii) the specific interactions of the NP with the different group density regions of the surface. While (i) promotes the random movement of the NP on the *xy* plane, (ii) increases the residence time of the NP in surface regions richer of receptors (stronger and more stable binding). The NP is seen to move over time toward higher-density group regions during the MD simulations. In this model, this is the effect of a kinetic asymmetry in the 2D *xy* diffusion of the NP on the surface, which makes the NP escape from high-density regions increasingly less favorable/probable. In particular, once the NP visits regions of the surface where the density of receptors is so high that $\Delta E_{ass} << \Delta E_{bind}$, on a long timescale for the NP it becomes more probable to disassemble rather than to escape from that region.

As shown in Figure 2, two different behaviors of NP are evident: in low-density regions, the NP globally preserves its spherical shape during the diffusion. Individual monomers can be eventually

lost during NP rolling, as the local receptor-monomer (receptor-ligand) interactions are stronger than the monomer-monomer interactions (see Supplementary Movie S1), but this does not perturb the integrity of the NP. On the other hand, in high-density receptors regions, the NP tends to deform, due to the increased multivalent interactions with many receptors on the surface. Even after the NP reaches the denser receptors region on the surface, the MetaD scheme keeps pushing the NP to change its *xy* position, which, in the last part of the CG-MetaD run, results into a NP disassembly/exfoliation.

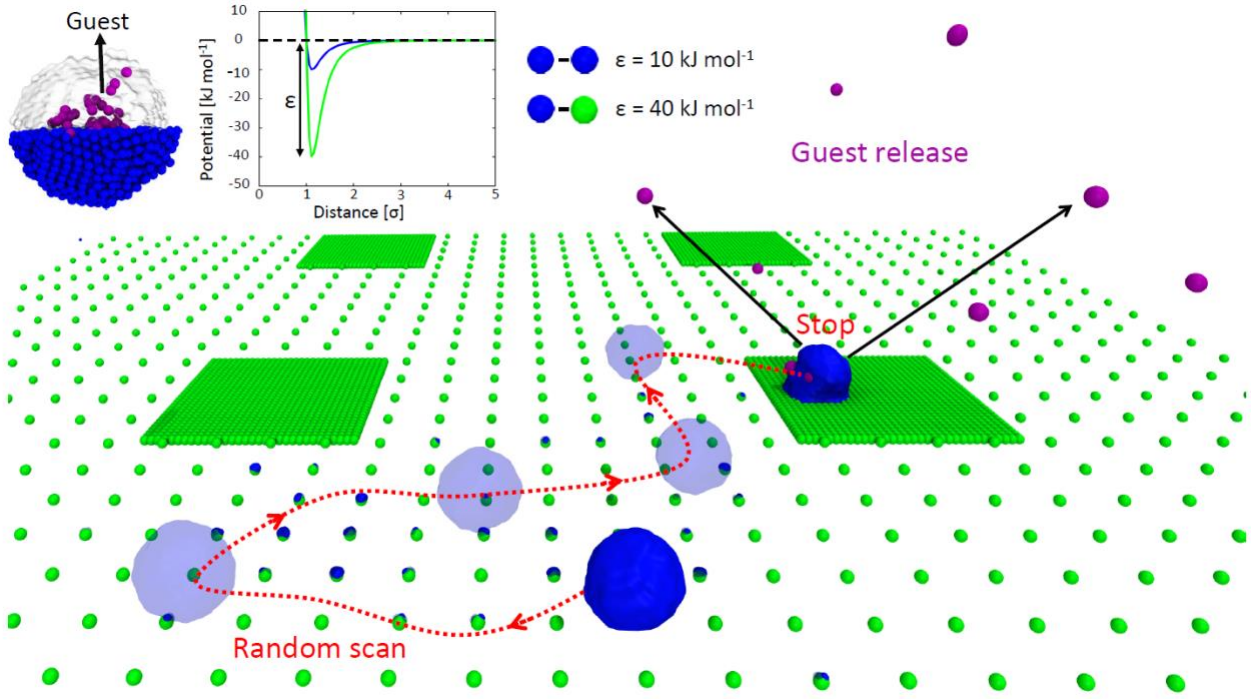

Figure 2. Simulating the density-responsive behavior of chemotactic NPs using minimalistic models. Minimalistic CG model of a supramolecular NP (blue CG beads: self-assembled monomers) with encapsulated guests (violet CG beads). In the surface model, two areas are distinguishable: with high and low receptor densities (green CG beads). Top: the ε values of the 12-6 LJ potentials in this model are tuned to have a ratio between the strengths of the monomer-monomer and monomer-receptor interaction ($\Delta E_{ass}/\Delta E_{bind}$ ratio) of ~¼. Bottom: CG-MetaD trajectory (red dotted arrows) showing NP rolling and diffusion on the surface. Starting from a receptor-poor region, the NP randomly explores the surface during the CG-MetaD run, until reaching a receptor-rich region. Once the NP binds a receptor-rich region of the surface, the MetaD simulation suggests that the presence of a force continuously pulling the NP may induce NP disassembly over time, and the consequent release the encapsulated guest particles (in violet).

Similar to experimental setups, in these *in silico* experiments we also encapsulate guest CG beads (Figure 2: in violet) within the NP, which weak interact with the other particles in the system (see Methods for details). Upon NP disassembly these are released in the surrounding environment (see Figure 2 and Supplementary Movie S1). It is worth noting that once the NP binds to the higher density region of the surface, the bias that keeps accumulaing during the CG-MetaD run increases rapidly (see Supplementary Figure S4). This confirms that, in a realistic system, once the NP reaches a surface region with a high-density of receptors, the probability for NP escape from it (as an entire assembled entity) drops dramatically. Moreover, the NP behavior seen late during the CG-MetaD also qualitatively suggests that the presence of eventual external forces (or stimuli), which keep acting on the NP attempting to move it away from such stably bound configurations, may eventually induce the breakage of the NP and the consequent release of the encapsulated guests. Such interesting hypothesis is tackled further in the next sections.

Higher-resolution insights into the effect of multivalent interactions. The preliminary evidence obtained through the minimalistic model of Figure 2 indicates that multivalent interactions (between the receptors on the surface and multiple ligands present on the NP) are key in controlling the chemotactic behavior of the NP on the surface. This suggests the intriguing perspective of controlling the autonomous behavior of the NP on the surface by rationally designing *a priori* the multivalent interaction between the self-assembled NP with the receptor-displaying surface. The minimalistic model of Figure 2 offers a flexible platform to monitor, *e.g.*, the effect of monomer-monomer interactions (assembly stability), the influence of receptor density

on the surface, or in general the impact of the relative strength of monomer-monomer vs. monomer-surface interactions on the behavior of the NP. However, the molecular resolution of this minimalistic model (one particle per-monomer) does not allow to obtain molecular-level information on how to practically control the NP chemotacticity. For example, it is known that a higher ΔE_{ass} would make the assembly more stable allowing in principle the entire NP to reach denser receptor regions. But what does this mean from a realistic, molecular point of view? How can one practically control ΔE_{ass}, ΔE_{bind}, and their ratio?

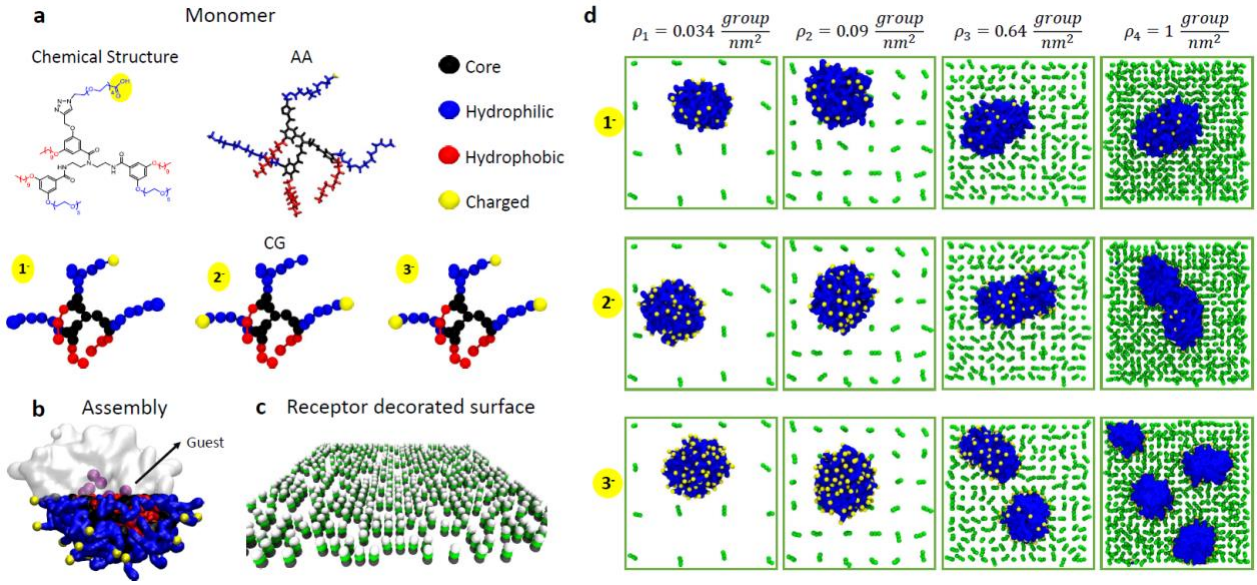

Figure 3. Submolecular resolution CG models to study self-assembled NPs and their adhesion onto functionalized surfaces. a) Chemical structure, all-atom (AA) and fine coarse-grained (CG) models of facially amphiphilic modular oligomers. These self-assembling units are composed of a branched core (in black), hydrophobic groups (red) which triggers self-assembly in aqueous solution, and hydrophilic groups (red), which can be functionalized in different ways (*i.e.*, with COO^- charged groups, in yellow, in the example studied herein). b) Fine CG model of a NP obtained via self-assembly of 44 oligomers in water. Guest CG particles (in purple) are incapsulated spontaneously in the NP, and used to monitor guest release upon eventual NP disassembly. c) CG model of a surface functionalized with +1*e* charged groups (dark green CG beads are constrained in their position, while the topmost white ones carry a +1*e* charge). d) CG-MD simulation of static NP adhesion to surfaces characterized by different densities of receptor groups. Snapshots taken after 1 μs of CG-MD showing NP destabilization and disassembly upon adhesion may be observed while increasing the charge densities on the surface and on the NP.

To answer such questions, a finer CG model description is necessary. As a second step, we thus moved to CG models of the system, where both the NP and the surface models are modeled with a ~5 Å resolution. Higher resolution molecular models enable to study the role of changing molecular structure of the self-assembling monomers, or *e.g.* of the multivalent interactions between the monomers and the receptors present on the surface. However, while becoming more realistic molecularly (*i.e.*, more chemically relevant), at the same time such sub-molecular resolution models become less general, as these have to refer to specific molecular structures.[35] As an example, here we use as a reference case facially amphiphilic oligomers that self-assemble in aqueous solution forming NPs, which were recently demonstrated to allow for successful encapsulation of hydrophobic guests in the NP interior.[13] Thanks to their intrinsic multivalent modular nature, these self-assembling oligomer units are ideal platforms for this study. They possess hydrophobic and hydrophilic groups that can be individually functionalized and changed. This allows, for example, to graft on their hydrophilic surface specific ligands (or chemical groups) that, exposed on the surface of the NP, allow to selectively bind determined receptors (or complementary chemical groups): changing the binding units and their number on the oligomer unit enables to tune the ΔE_{bind}. The use of such oligomers also opens the opportunity to modify the hydrophobic groups,[36] making the assembly more/less stable, changing the ΔE_{ass}. Previous studies by our group demonstrated that molecular models can provide useful insight in such assemblies and in their stimuli-responsive behavior.[36–40] In detail, the self-assembling oligomers that we employ here as a reference platform (Figure 3a) are composed of a branched scaffold, three hydrophobic decyl chains (hydrophobic face), and three hydrophilic polyethylene glycol moieties (hydrophilic face). Variable functionalities can be grafted onto the hydrophilic surface groups of these oligomers, which remain ex-posed on the NP surface upon oligomers self-assembly.[13,37,39]

In this case, we consider oligomers displaying a variable number of carboxylic acid functionalities (COOH groups). These are deprotonated at neutral pH (1, 2, and 3 COO^{-}), allowing to impart a charge of -1*e*, -2*e*, or -3*e* to the oligomers (Figure 3a). As seen in preliminary experimental evidence, this allows to obtain negatively charged self-assembled oligomer NPs (see Figures S1-S2), capable of binding to positively-charged surfaces (Figure S3). First, we developed all atom (AA) models for these oligomers. We characterized (i) the behavior of a single oligomer in aqueous solution via AA-MD simulations. We also used AA-MetaD simulations to evaluate (ii) the oligomer-oligomer dimerization free-energy, estimating the strength of the interactions between the oligomers in solution (see Figure S5 in the Supplementary Information). We then developed fine CG models for the oligomers (resolution ~5 Å, with a 3-4:1 heavy-atoms:CG-particle mapping), based on the widely used MARTINI force field scheme.[41] In particular, given the spatiotemporal scales associated to the phenomena of interest herein, we considered the same protocol to develop and optimize an implicit-solvent version of these CG models based on the dry-version of the MARTINI force field.[42] First, we used the Swarm-CG software[43] to optimize the bonded terms in the CG model and hence to reproduce (i), second, the MARTINI bead types have been adjusted to obtain via CG-MetaD simulations dimerization free-energy profiles (ii) consistent with those obtained using the AA models (see Methods, and Figure S5). [28,38,44] With this implicit-solvent fine CG model, we obtained via self-assembly a NP model composed of 44 oligomers, spontaneously sequestering from the solution, and encapsulating 10 CG guest beads (Figure 3b, violet) during a CG-MD simulation. We also developed a model of a flat surface decorated with positively charged CG groups. The receptor groups are modeled as 3 CG beads, where the bottom one is constrained in its position, and the topmost one is +1*e* charged (Figure 3c). Four surface densities have been modeled (ρ_1, ρ_2, ρ_3, ρ_4), up to a maximum density of ρ_4 = 1 +charged-

group/nm^2 (Figure 3d), in the order of experimentally reported density values for amino-grafted surfaces.[45–48] Complete details on the parametrization of the AA and CG models are provided in the Methods section. We used these CG models to study the NP adhesion on the surface. In particular, we were interested to observe the behavior of the NP following to the adhesion to the surface (in line to the hypothesized scheme of Figure 1b). CG-MD simulations of NPs composed of oligomers bearing 1, 2 or 3 COO^- charged groups (total NP charge of -44*e*, -88*e* and -132*e* respectively) binding surface models with growing densities of receptor groups (Figure 3d: from ρ_1 to ρ_4) clearly show that the behavior of the NP upon binding is strictly related to the strength of the multivalent NP-surface interactions, which depends on the density of charges present on the target surface, ρ, and on the NP (number of COO^- charged groups). Shown in Figure S6 (see Supplementary Information), the NP adhesion to the surface in-creases moving from monovalent to trivalent self-assembled oligomers, as it is shown by the number of NP beads in contact with the surface receptor groups. Such evidence from the models also finds confirmation in Structural Illumination Microscopy (SIM) experiments, showing an increment of signal related to surface bound NPs while increasing the multivalent interactions (see Figure S1 and Figure S2 of the Supplementary Information). Noteworthy, the contacts between the oppositely charged groups of the NP and of the surface reach a maximum of ~132 in the case of surface density ρ_4 and trivalent NP oligomers, where complete NP disassembly can be observed during the CG-MD simulation (Figure 3d: bottom-right snapshot). While these results indicate that the strength of the NP-surface binding can be in general strengthened or weakened by playing either with the NP multivalent charges or with the surface distribution of receptor groups, unbiased CG-MD simulations were found ineffective to study the dynamic behavior of the NPs after surface binding (*e.g.*, in cases where the NP does not break-up upon adhesion). In particular, we used multiple infrequent CG-

MetaD simulations to obtain qualitative information on the characteristic timescale for NP unbinding from a monovalent interaction with one positively charged surface group (see Methods for details). Analysis of the infrequent CG-MetaD simulations shows that the breakage of a monovalent electrostatic interaction between one -1e charged group in the NP and one +1e charged group on the surface requires crossing a free-energy barrier of ~6.5 kcal mol^{-1} on average, with a characteristic escape/unbinding time of ~1.14 ms (~1011 simulation timesteps, τ) at room temperature (see Figure 4a and Figure S7 in the Supplementary Information). While transition times extracted from such simplified CG models must be considered as purely qualitative, it is worth noting that escaping from multivalent interactions with the surface by the NP can be only slower than this, indicating that the study of the dynamics of the NP after its binding to the surface far-exceed the possibilities of classical MD simulations. To obtain an insight on the behavior of the system after the binding between the NP and the surface has occurred, we thus turned again to MetaD simulations. Accelerating the NP dynamics on the surface using a gaussian-like bias potential on the *xy* position of the NP center of mass, allowed us to obtain qualitative insight on the diffusion behavior of the NP after binding to the surface. We carried out 36 multiple-walker CG-MetaD simulations starting from a configuration where the NP is placed in a lowest receptor-density region and activating the NP *xy* exploration of the surface (Figure 2). Allowing to explore longer timescales, these CG-MetaD simulations confirmed that the NP tend to move away from the lowest density regions at room temperature (see Supplementary Movie S2 for one example CG-MetaD trajectory). This is consistent with preliminary microscopy experiments showing that movement after surface binding of NPs based on the same chemistry is possible (see Figure S1 in the Supplementary Information).

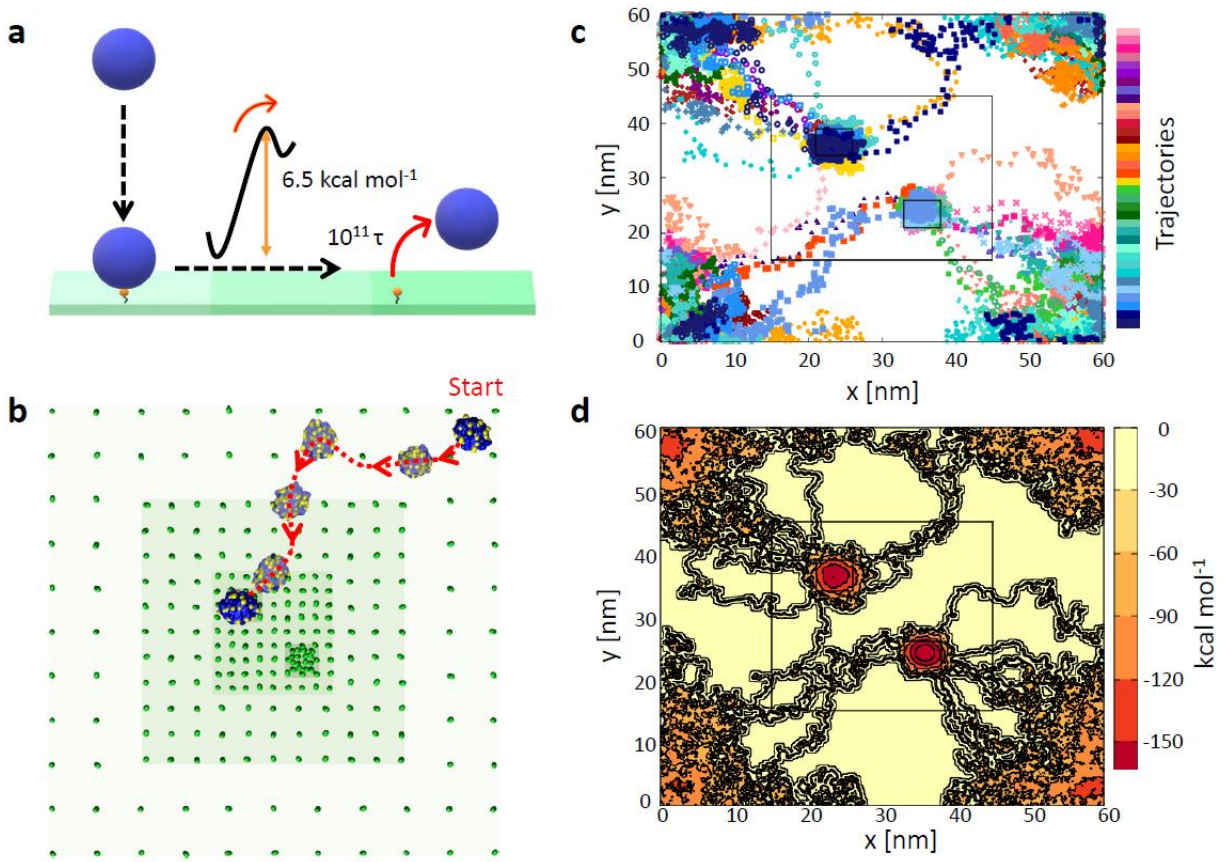

Figure 4: Submolecular CG models of NP chemotaxis. a) Free-energy barrier and characteristic escape timescale (expressed in simulation timesteps, τ) for NP unbinding from the surface in the case of a monovalent interaction. b) An example of CG-MetaD trajectory extracted from the ensemble of panel (c,d). c) All the trajectories of the 36 multiple-walker CG-MetaD simulations. Every color represents a different CG-MetaD simulation. d) Energy landscape obtained from 36 multiple-walker CG-MetaD simulations. In all CG-MetaD runs, the NPs tend to diffuse following the chemical gradient, from lowest to highest-density regions on the surface, from where the simulations indicate that it is difficult for the NP to escape.

From these 36 CG-MetaD simulations we also calculated the energy associated to each configuration visited by the NP. Although obtaining satisfactory convergence in such MetaD simulations is prohibitive, even on a purely qualitative level, the data of Figure 4b suggest that the NP escape from the highest density regions on the surface requires crossing a very high free-energy barrier. As seen in Figure 2 using the minimalistic NP model, also in this case the CG-MetaD

simulations indicate that such NP are keen to reach higher-density regions over time, showing an extremely low probability to escape from the strong multivalent binding that are established in these regions (Figure 4d). It is interesting to note that in this finer CG model, the NP-surface binding is mainly driven by electrostatic interactions, while in the minimalistic model of Figure 2 this is controlled by Van der Waals interactions (expressed by LJ potentials). Electrostatic interactions modeled via such simplified CG models should be handled with care, and the results obtained with these simulations have a purely qualitative purpose (see also Methods section). Nonetheless, it is worth noting that consistent NP behaviors are observed in either cases, independently on the type of interaction that govern the specific NP-surface binding. This suggests that the autonomous migration of such chemotactic NPs following chemical surface gradients has a general character. In particular, rather than to the specific type of interaction, this again appears to be ascribable to the kinetic asymmetry introduced in the system by the increased/decreased multivalent interactions established by the NP in higher/lower density regions of the surface.

Towards the rational design of density-responsive chemotactic NPs. The previous sections suggest that it is possible, in principle, to design synthetic NPs that can follow chemical gradients on a surface, and that can stop once a determined density is met. In the perspective of mimicking the fascinating chemo-tactic properties seen in Nature, next questions are whether it is possible also to control the NP disassembly, and the re-lease of the encapsulated guests, once a critical surface concentration is encountered, and eventually how. To challenge these points, we designed in silico experiments using our fine CG models. In detail, we built a CG model of a longitudinal surface functionalized with positively charged groups whose density grows along the main surface dimension (Figure 5a: from ρ_0 to ρ_3). One NP is initially placed in the $\rho 0$, receptor-free region of

the surface (Figure 5a, left). We then ran CG-MD simulations where a constant force is applied to the center of mass of the NP, continuously pushing the NP along the chemical surface gradient vector (*i.e.*, from lower to high-er density regions of +1e surface groups). The magnitude of the force was set in order to mimic the effect on the NP of an external flux comparable to that present in e.g. blood vessels (i.e. an NP directional diffusion rate of ~0.5-1 cm/s, see Methods for details).[49] In some cases, we could observe the NP assembly was pushed by the force until reaching a complete break-up and release of the encapsulated guests (Figure 5a), while in other cases the NP was seen to deform without disassembling during the surface rolling (see Supplementary Movies S3, S4, S5). NP disassembly and deformations were mainly monitored by evaluating the variations of the NP Solvent Accessible Surface Area (SASA) during the CG-MD run.

The results show that the NP tends to establish a higher number of multivalent interactions with the surface groups while moving towards denser surface regions, as recently demonstrated with fluorescent microscopy experiments in other multivalent binding systems[19]. Such enhancement of the multivalent binding with the surface leads to an increased exposure of the hydrophobic parts of the NP oligomers to the solvent, thereby entailing an increase of the SASA of the assembly (ΔSASA). The ΔSASA increases even further as a consequence of NP exfoliation, as well illustrated in Figure 5b (left). Interestingly, increasing the number of charges on the oligomer surface (*i.e.*, enhancing the NP multivalency), the NP disassembly occurs earlier, at lower surface densities of receptor groups (Figure 5b, left). The number of contacts between the encapsulated guest CG particles and the oligomers in the NP also provide indication on the stability of the guest encapsulation and of their eventual release. In particular, by calculating the extent of the drop in the guest-oligomer contacts during the CG-MD runs, we can estimate the percentage of guest release as a function of the surface density of receptors (ρ). Shown in Figure 5b (right), the guest

release is associated to the NP disassembly. Our simulations clearly show that by modulating the number of charges on the oligomers it is possible to trigger the release of the guests, and in principle also to control at which receptor density this takes place.

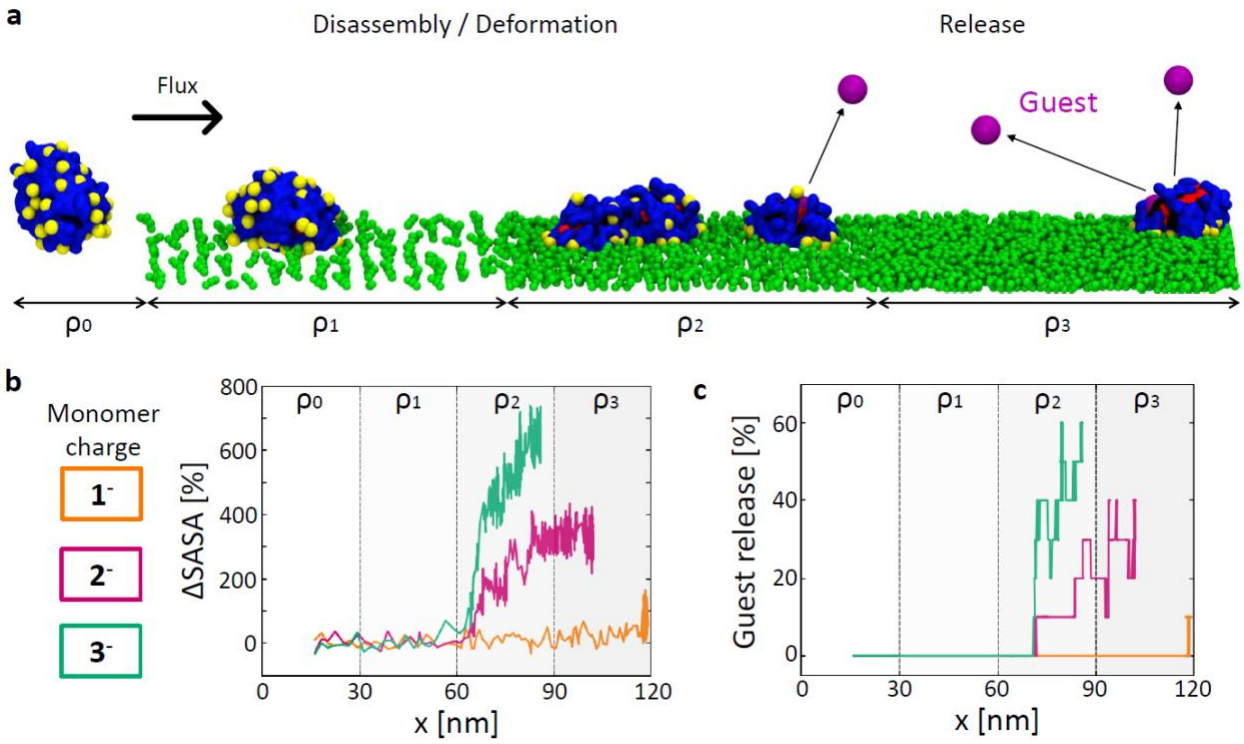

Figure 5. *In silico* experiments of NP rolling, disassembling and guest releasing in the presence of an external flux. a) CG-MD simulation setup. b,c) Monitoring NP disassembly and guest release. b) Percentage variation of the NP SASA (ΔSASA) for the NPs as a function of the oligomer charge. c) Percentage of guest release as a function of the oligomer charge.

The identification of a threshold receptor density as function of multivalent interactions has been recently estimated by a sophisticated image post-processing approach[19]. However, perhaps the main advantage of these self-assembling oligomers in their modular structure, opens the possibility of fine-tuning the hydrophobic/hydrophilic groups in order to control the NP disassembly and the release of the guests during the NP chemotaxis. While the $\Delta E_{ass}/\Delta E_{bind}$ ratio is critical to control

the chemotactic responsive behavior of the NPs, our simulations highlight how such a control can be achieved by *e.g.* modulating the multivalent interactions between the NP and the sur-face, or even by changing the number of -1*e* charged groups on the oligomers (namely, changing the $\Delta E_{ass}/\Delta E_{bind}$ by acting on the ΔE_{bind}). However, the $\Delta E_{ass}/\Delta E_{bind}$ ratio may be modified also by altering the hydrophobic groups in the oligomers. This has been recently done for similar self-assembling oligomers, showing remarkable effects on the temperature-responsive behavior of the NPs that these form.[36] As a further proof of concept, we thus studied the effect of changing the hydrophobic moieties in the oligomer units on the NP chemotaxis. Considering the reference oligomer of Figures 3-4 (named Original in Figure 6a), we systematically replaced its C10 hydrophobic units. Shown in Figure 6b, we obtained a Type-1 monomer variant by adding four carbon units (C14), *i.e.*, the equivalent of 1 hydrophobic CG bead in our CG model. A Type-2 monomer variant carries a halogenated carbon group (orange) at the end of the Original structure, making the hydrophobic tails of the oligomers more hydrophilic compared to the Original saturated alkyl chains. Finally, we substituted the last CG bead in the decyl tails of the Original oligomer with phenyl and naphthyl functional groups, obtaining respectively Type-3 or Type-4 oligomer variants (Figure 6b). It is worth noting that the two last modifications affect not only the aggregation strength, but also the assembly shape, due to different packing interactions between the cyclic functional groups.

As a proof of concept, we repeated the *in silico* experiments of Figure 5, running out-of-equilibrium CG-MD simulations for the Types 1-4 oligomers (carrying a variable amount of charges on the hydrophilic groups: -1*e*, -2*e*, -3*e*), and compared the behavior of these to the Original NPs (Figure 6). Figure 6c displays the comparison between the new NP variants compared to Original reference one. Since Type-1, Type-3 and Type-4 are more hydrophobic than the

Original oligomer, their NPs are more stable. In Type-1 and Type-3 NP variants, the complete disassembly/exfoliation takes place only at density ρ_3, where the multivalent interactions with the surface are stronger than in ρ_2, where the Original -3e NP disassembles (Figure 6c, left: ΔSASA data). Again, we observe that the percentage of guest is consequent and follows the NP disassembly (Figure 6c, right). Interestingly, in Type-4 the monomer-monomer interaction is so strong that this NP variant deforms at higher ρ, but it does not disassemble (no guest release) at any receptor density (ΔE_{ass} prevails on ΔE_{bind}). Similar data are reported for all -1e and the -2e NP variants in the Supplementary Information (see Figures S8 and S9). These results clearly demonstrate that the strength of the NP-surface interaction is not the unique important factor, but the $\Delta E_{ass}/\Delta E_{bind}$ balance (thus controllable also by changing the ΔE_{ass}) is the key parameter controlling the behavior of these NPs. To this regard, Figure 6d clearly shows how comparable behaviors in the system can be obtained with different NPs. While these cases change both in the hydrophobic groups and in the number of NP binding charges, evidently such combinations produce comparable global $\Delta E_{ass}/\Delta E_{bind}$ balances in the NPs, which makes them behaving on the surface in similar way. It is interesting to note, for example, how Types-1 and Types-3 NPs composed of -1e charged oligomers do not disassembly and do not release guests during the CG-MD runs, be-having in the same way of Type-4 -2e charged NP. While the former NPs are less tightly assembled, the latter NP is more stable (stronger ΔE_{ass}), thus requiring a stronger interaction with the surface (stronger ΔE_{bind}) to behave in comparable way. The perspective provided by these in silico investigations is quite neat and intriguing, as it suggests that once the density of receptors on a surface is known, it is in principle possible to rationally design the NP to control at what density this will disassemble and will release the encapsulated guests in the presence of an external

flux (or at what density the NP would simply stop in the absence of any flux – see Figure 2 and Figure 4).

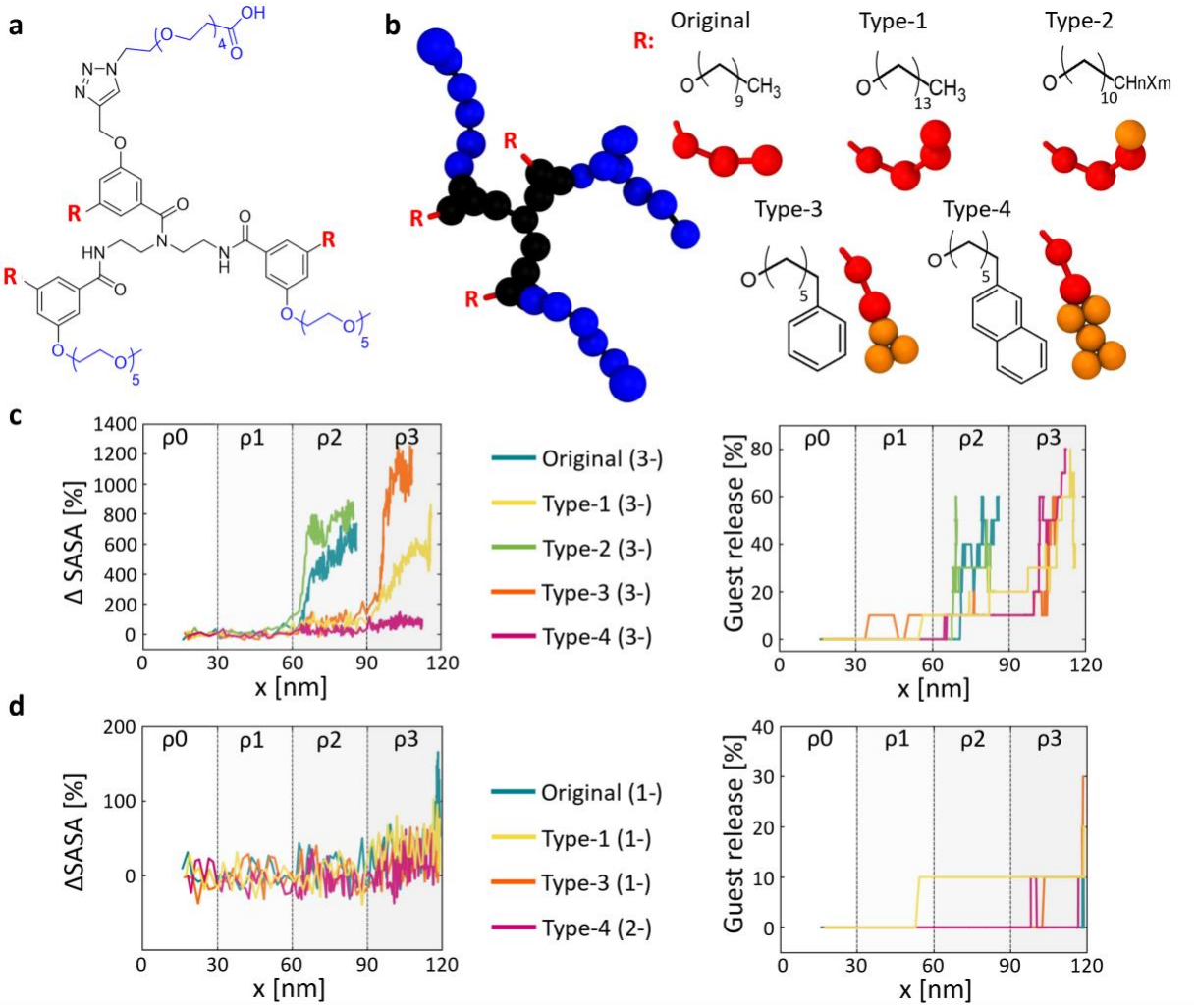

Figure 6. Modulating the NP chemotaxis and responsiveness by modulating the hydrophobicity of the self-assembling units. a) The Original reference oligomer (C10 hydrophobic tails). b) Hydrophobic groups of the Type-1, Type-2, Type-3 and Type-4 oligomer variants and their corresponding CG models. c) Comparison of ΔSASA (NP SASA variation) and percentage of guest release for NPs composed of the different trivalent (-3e) oligomer variants. Same data for the (-2*e*) NP variants are reported in the Supplementary Information (see Figures S8 and S9). d) Similar NP behaviors can be obtained by NPs composed of oligomer variants having a similar $\Delta E_{ass}/\Delta E_{bind}$ balance.

CONCLUSION

In this work we have designed a concerted computational strategy to investigate supramolecular NPs with interesting chemotactic and density-responsive bioinspired properties. We have used a combination of multiscale molecular models and advanced simulation approaches to track, monitor, and ultimately to understand the dynamic behavior of the self-assembled NPs on receptor-grafted surfaces. Moving from minimalistic to finer CG models, we have uncovered the physical basis that controls the chemotactic behavior of the NP. First, we have unveiled the key role played by the competition between the self-assembly stability of the NP (ΔE_{ass} energy) and the strength of the interaction between the NP and the surface (ΔE_{bind} energy). Such ΔE_{ass} *vs.* ΔE_{bind} competition controls the autonomous motion of the NP along chemical gradients and also the fate of the NP. Secondo, using soft NPs made of modular self-assembling multivalent oligomers as an example case study, we provided chemical relevance to our results, showing chemical routes to achieve controlled bioinspired chemotaxis in artificial self-assembled systems. In fact, by tuning the NP surface charges and the chemical structure of the monomer units (*e.g.*, the nature of the hydrophobic groups in the self-assembling oligomers) it is possible in principle to control how the NP binds to the surface, its spontaneous diffusion on surface chemical gradients, its rolling, stopping, and, in the case of an external stimulus (*i.e.*, a flux), even NP disassembly and guest-release in controlled spots of the surface. The results discussed here-in suggest that such in silico experiments can be extremely valuable for augmenting our understanding of how to customize the structure of the self-assembling units to control the stability of the NP, the $\Delta E_{ass}/\Delta E_{bind}$ balance, and the dynamic behavior of these chemotactic NPs. Furthermore, we show that it is in principle possible, once the features of a target surface are known, to rationally design or customize ad hoc the NPs in order to achieve controllable chemotaxis in artificial molecular systems.

MATERIALS AND METHODS

All simulations were conducted using GROMACS 2018.6[50,51] patched with PLUMED 2.5[52]. The VMD visualization suite was used to display and render the simulated systems.

Minimalistic coarse-grained model and simulations.

The minimalistic CG model is characterized by three different bead types representing: (i) the monomers within the assembly, (ii) the guest particles contained inside the self-assembled NP, and (iii) the receptors grafted on the surface. The interactions have been defined using a Lennard Jones (LJ) 12-6 potential, initially setting the LJ parameters to $\sigma = 0.47$ nm and $\varepsilon = 10$ kJ mol^{-1}, for the monomer-monomer interactions (ΔE_{ass}) and to $\sigma = 0.35$ nm and $\varepsilon = 40$ kJ mol^{-1} for the monomer-receptor interaction (ΔE_{bind}), obtaining a $\Delta E_{ass}/\Delta E_{bind}$ ratio of ~¼ comparable to that recently estimated in the case of similar self-assembling oligomers containing a ligand capable of specifically bind to a complementary receptor protein (based on the avidin-biotin interaction).13 We also added on the surface a weakly attractive potential of 2.0 kJ mol^{-1} (20 times weaker than specific interactions), in order to mimic the weak non-specific interactions between the NP and the surface and to prevent the NP to penetrate inside the surface in receptor-free surface regions. In this simplified model, the surface receptor CG beads were kept frozen during the simulations. The NP-surface system was initially minimized using a steepest descent algorithm, and a leap-frog stochastic dynamics integrator was used for the production run. A Langevin dynamics was conducted using Coulomb and Van der Waals cutoffs of 1.1 nm, and a relative dielectric constant of $\varepsilon_r = 15$ (to implement electrostatic screening of the solvent, accordingly with the Dry MARTINI force field standards).[42] All simulations using this model have been conducted at 300 K of

temperature, in NVT conditions (constant N: number of particles, V: volume, T: temperature) using a 20 fs timestep. Due to the anisotropic nature of the system, Periodic Boundary Conditions were considered only along *x*- and *y*-axis. Metadynamics (MetaD) simulations were used to enhance the NP sampling of the surface. A MetaD bias was applied on the x- and y-distances (used as the collective variable, CV) of the NP center of mass respect to the origin of the system, depositing every 5000 steps Gaussian kernels of height 20 kJ/mol^{-1} and width of 1.0 for both variables.

Submolecular resolution models and simulations

AA and fine CG models. The atomistic model was built with Avogadro[53] based on the chemical structure of the oligomers. The oligomers were created as composed of three main parts (hydrophobic tails, hydrophilic tails and core), which have been parametrized based on the General AMBER Force Field (GAFF),[54] using Antechamber[55]. The fine CG models of the oligomers were built based on the MARTINI force field.[41] The bonded parameters have been optimized automatically to reproduce the bond, angle and dihedral distributions of the AA-MD simulations using Swarm-CG[43]. The non-bonded parameters have been optimized by choosing the appropriate MARTINI bead types in order to (i) reproduce the radius of gyration and the Solvent Accessible Surface Area (SASA) of the all-atom model seen in AA-MD simulations, and (ii) to reproduce the free-energy of dimerization between two oligomers in water obtained via metadynamics (AA-MetaD *vs.* CG-MetaD) simulations between two monomers (see Figure S5 in the Supplementary Information). For the best reliability, first a wet MARTINI-based CG model was created and optimized, which has been then used to optimize the Dry MARTINI-based CG model used for the simulations of Figures 3-6. The self-assembled NPs were obtained by inserting a large number of dry-CG monomers in a box and a classical MD simulation was run. The larger and more stable NP

was found composed of 44 monomers and was used as a reference in all the simulations. That number of repetitive self-assembled units was found to give optimal results between the NP size and shape, without affecting the simulation performances. Ten CG beads were added inside the aggregate in order to represent guest particles. The interaction between such guest particles is weak enough to allow the prompt monitoring of their release in case of the NP's disassembly (σ = 0.43 nm and ε = 6.5 kJ mol^{-1} The alkylamine groups on the surface were also modeled at the same resolution level based on the Dry MARTINI force field. In detail, the amino-groups are defined by three CG beads: a base one, grafted to the surface, a central CG bead (mimicking a car-bon linker), and a charged hydrophilic head. In order to keep the receptor position fixed, the base CG beads of the receptor groups were kept frozen during the simulations. Complete structures and parameters for all CG models used here-in are available at https://github.com/GMPavanLab/RollingNP/.

Unbiased simulations. Since all the simulations were per-formed in implicit solvent, the relative dielectric constant was set to ε_r = 15 to model the electrostatic screening of the solvent (standard for the Dry MARTINI force field).[42] All CG-MD simulations were run in NVT conditions (constant N: number of particles, V: volume, T: temperature) at T = 300 K. All the systems were preliminary minimized using a steepest descent algorithm and a leap-frog stochastic dynamics integrator was then used for all unbiased MD pro-duction runs, using a 20 fs timestep, and Coulomb and Van der Waals cutoffs of 1.1 nm. For the CG-MD simulations of the static NP adhesion on different receptor density regions (Figure 3d), the different NP model has been initially centered on top of four different 20 x 20 nm^2 surfaces characterized by four different densities: ρ_1 = 0.034 rec/nm^2, ρ_2 = 0.09 rec/nm^2, ρ_3 = 0.64 rec/nm^2 and ρ_4 = 1 rec/nm^2, while each system was then equilibrated for 1 μs of CG-MD simulation.

Infrequent MetaD simulations for the study of NP un-binding/escape. We ran 30 infrequent CG well-tempered MetaD simulations to obtain information on the characteristic timescale and the associated free energy barrier that has to be crossed in the system to detach a NP (composed of -1e self-assembled oligomers) bound to a single surface receptor (Figure 4a). In these runs, as the CV we used the number of contacts between the NP's charged beads and the surface receptor CG beads. We used a bias factor of 10, a gaussian height of 1.2 kJ mol^{-1}, a deposition stride of 1 gaussian every 50000 timestep with a sigma of 0.5 nm. Simulations were terminated once the number of contacts is 0. The characteristic timescale for the event was calculated from the poissonian fit of the unbiased transition times distributions obtained from the 30 infrequent MetaD runs. The unbiased transition time (t) can be calculated from each individual MetaD run as:

$$t = t_{MetaD}\left\langle e^{\beta(V(s(R),t))}\right\rangle_{MetaD}$$

where V(s(r),t) is the time dependent bias provided for the transition during the run, the exponential (brackets) is averaged over the MetaD run and β is kT^{-1} . The transition times (t) calculated from the MetaD runs for were then used to build the transition probability distribution $P_{n\geq1}$ (namely, the probability to observe at least one exchange event by time t:

$$P_{n\geq1} = 1 - e^{\frac{-t}{\tau}}$$

where τ is the characteristic time for rare events. Figure S7 shows the exchange times collected from the individual runs. These fit well with poissonian transition probability distributions $P_{n\geq1}$. It is possible to calculate the characteristic timescales (TAU: τ) for exchanging one monomer from the fiber's tip in both systems.

Multiple-walker CG-MetaD simulations. In the multiple-walker MetaD simulations, the surface was characterized only by the four central areas measuring 60 x 60 nm^2. Multiple-walker MetaD was used to explore in parallel 36 simulations of the same CG system. The bias acted along the *x*- and *y*-distance of the NP's center of mass from to the origin of the system. The bias was constructed by depositing every 500 CG-MD steps Gaussian kernels of height 1.2 kJ mol^{-1} and width of 0.1 for both variables. Repeating the simulations with or without using the Particle Mesh Ewald (PME) summation to treat long-range electrostatics provided consistent results, proving the general validity of the approach in exploring the chemotactic NP behavior on the surface.

***In silico* NP rolling and exfoliation experiments.** We built a surface model having size 120 x 30 nm^2, characterized by four consecutive receptor density regions: ρ_0 = 0 rec/nm^2, ρ_1 = 0.12 rec/nm^2, ρ_2 = 0.52 rec/nm^2, ρ_3 = 1.12 rec/nm^2, 30 x 30 nm^2 each (see Figure 5a). In these CG-MD simulations, we used the same NPs composed of 44 assembled oligomers used in Figures 2 and 3. The CG-MD runs were conducted in NVT conditions at the temperature of 300 K, while Coulomb and Van der Waals interactions were modelled using a 1.1 nm cutoff. During these MD runs, a constant force F = -100 kJ mol^{-1} nm^{-1} was applied on the center of mass of the NP, directed along the main x-axis of the surface (Figure 5a), in order to obtain a pulling effect on the NP comparable to that of a flux similar to that existing on the blood vessels (NP diffusion rate: ~0.5-1 cm/s).[49] To avoid NP jumping far from the surface in the (receptor-free) region, a wall on z-axis was added using the PLUMED plugin on the center of mass of the NP at 5 nm with kappa=150.0 and exp=2.

ASSOCIATED CONTENT

Supporting Information concerning the input files used for the simulations, the molecular models, as well as additional data from the simulations is available in the Supporting Information and on: https://github.com/GMPavanLab/RollingNP/.

AUTHOR INFORMATION

Corresponding Author

* giovanni.pavan@polito.it

ACKNOWLEDGMENT

G.M.P. acknowledges the support received by the Swiss National Science Foundation (SNSF grant 200021_175735) and by the European Research Council (ERC) under the European Union's Horizon 2020 research and innovation program (grant agreement no. 818776 – DYNAPOL). The authors also acknowledge the U.S. Army Research Office (grants W911NF-18-1-0355 and W911NF-15-1-0568) for supporting this work. The authors also thank the computational resources provided by the Swiss National Supercomputing Center (CSCS) and by CINECA.

REFERENCES

(1) De Oliveira, S.; Rosowski, E. E.; Huttenlocher, A. Neutrophil Migration in Infection and Wound Repair: Going Forward in Reverse. *Nat. Rev. Immunol.* **2016**, *16*, 378–391

(2) Stuelten, C. H.; Parent, C. A.; Montell, D. J. Cell Motility in Cancer Invasion and Metastasis: Insights from Simple Model Organisms. *Nat. Rev. Cancer* **2018**, *18*, 296–312

(3) Trepat, X.; Wasserman, M. R.; Angelini, T. E.; Millet, E.; Weitz, D. A.; Butler, J. P.; Fredberg, J. J. Physical Forces during Collective Cell Migration. *Nat. Phys.* **2009**, *5*, 426–430

(4) Tambe, D. T.; Corey Hardin, C.; Angelini, T. E.; Rajendran, K.; Park, C. Y.; Serra-Picamal, X.; Zhou, E. H.; Zaman, M. H.; Butler, J. P.; Weitz, D. A.; et al. Collective Cell Guidance

by Cooperative Intercellular Forces. *Nat. Mater.* **2011**, *10*, 469–475

(5) Roca-Cusachs, P.; Sunyer, R.; Trepat, X. Mechanical Guidance of Cell Migration: Lessons from Chemotaxis. *Curr. Opin. Cell Biol*. **2013**, *25*, 543–549

(6) Datta, S.; Kato, Y.; Higashiharaguchi, S.; Aratsu, K.; Isobe, A.; Saito, T.; Prabhu, D. D.; Kitamoto, Y.; Hollamby, M. J.; Smith, A. J.; et al. Self-Assembled Poly-Catenanes from Supramolecular Toroidal Building Blocks. *Nature* **2020**, *583*, 400–405

(7) Mishra, A.; Dhiman, S.; George, S. J. ATP-Driven Synthetic Supramolecular Assemblies: From ATP as a Template to Fuel. *Angew. Chem. Int. Ed.* **2021**, *60*, 2740–2756

(8) Yan, X.; Wang, F.; Zheng, B.; Huang, F. Stimuli-Responsive Supramolecular Polymeric Materials. *Chem. Soc. Rev.* **2012**, *41*, 6042–6065

(9) Aida, T.; Meijer, E. W.; Stupp, S. I. Functional Supramolecular Polymers. *Science*. **2012**, 335, 813–817

(10) Xu, F.; Pfeifer, L.; Crespi, S.; Leung, F. K. C.; Stuart, M. C. A.; Wezenberg, S. J.; Feringa, B. L. From Photoinduced Supramolecular Polymerization to Responsive Organogels. *J. Am. Chem. Soc.* **2021**, *143*, 5990–5997

(11) Bochicchio, D.; Kwangmettatam, S.; Kudernac, T.; Pavan, G. M. How Defects Control the Out-of-Equilibrium Dissipative Evolution of a Supramolecular Tubule. *ACS Nano* **2019**, *13*, 4322–4334

(12) Roy, I.; Bobbala, S.; Young, R. M.; Beldjoudi, Y.; Nguyen, M. T.; Cetin, M. M.; Cooper, J. A.; Allen, S.; Anamimoghadam, O.; Scott, E. A.; et al. A Supramolecular Approach for Modulated Photoprotection, Lysosomal Delivery, and Photodynamic Activity of a Photosensitizer. *J. Am. Chem. Soc.* **2019**, *141*, 12296–12304

(13) Amado Torres, D.; Garzoni, M.; Subrahmanyam, A. V.; Pavan, G. M.; Thayumanavan, S.

Protein-Triggered Supramolecular Disassembly: Insights Based on Variations in Ligand Location in Amphiphilic Dendrons. *J. Am. Chem. Soc.* **2014**, *136*, 5385–5399

(14) Zarzar, L. D.; Aizenberg, J. Stimuli-Responsive Chemomechanical Actuation: A Hybrid Materials Approach. *Acc. Chem. Res.* **2014**, *47*, 530–539

(15) Semenov, S. N.; Kraft, L. J.; Ainla, A.; Zhao, M.; Baghbanzadeh, M.; Campbell, V. E.; Kang, K.; Fox, J. M.; Whitesides, G. M. Autocatalytic, Bistable, Oscillatory Networks of Biologically Relevant Organic Reactions. *Nature* **2016**, *537*, 656–660

(16) Cui, J.; Daniel, D.; Grinthal, A.; Lin, K.; Aizenberg, J. Dynamic Polymer Systems with Self-Regulated Secretion for the Control of Surface Properties and Material Healing. *Nat. Mater.* **2015**, *14*, 790–795

(17) Liu, J.; Xu, H.; Tang, X.; Xu, J.; Jin, Z.; Li, H.; Wang, S.; Gou, J.; Jin, X. Simple and Tunable Surface Coatings via Polydopamine for Modulating Pharmacokinetics, Cell Uptake and Biodistribution of Polymeric Nanoparticles. *RSC Adv.* **2017**, *7*, 15864–15876

(18) Liao, Y. H.; Lin, C. H.; Cheng, C. Y.; Wong, W. C.; Juo, J. Y.; Hsieh, C. L. Monovalent and Oriented Labeling of Gold Nanoprobes for the High-Resolution Tracking of a Single-Membrane Molecule. *ACS Nano* **2019**, *13*, 10918–10928

(19) Overeem, N. J.; Hamming, P. H. (Erik); Tieke, M.; van der Vries, E.; Huskens, J. Multivalent Affinity Profiling: Direct Visualization of the Superselective Binding of Influenza Viruses. *ACS Nano* **2021**, *15*, 8525–8536

(20) Di Iorio, D.; Huskens, J. Surface Modification with Control over Ligand Density for the Study of Multivalent Biological Systems. *ChemistryOpen* **2020**, 9, 53–66

(21) Yue, Y.; Gao, Y.; Yu, Y. "Waltz" of Cell Membrane-Coated Nanoparticles on Lipid Bilayers: Tracking Single Particle Rotation in Ligand-Receptor Binding. *ACS Nano* **2018**,

12, 11871–11880

(22) Taylor, R. W.; Mahmoodabadi, R. G.; Rauschenberger, V.; Giessl, A.; Schambony, A.; Sandoghdar, V. Interferometric Scattering Microscopy Reveals Microsecond Nanoscopic Protein Motion on a Live Cell Membrane. *Nat. Photonics* **2019**, *13*, 480–487

(23) Wang, M.; Ravindranath, S. R.; Rahim, M. K.; Botvinick, E. L.; Haun, J. B. Evolution of Multivalent Nanoparticle Adhesion via Specific Molecular Interactions. *Langmuir* **2016**, *32*, 13124–13136

(24) Lin, L.; Zeng, X. Computational Study of Cell Adhesion and Rolling in Flow Channel by Meshfree Method. *Comput. Methods Biomech. Biomed. Engin.* **2017**, *20*, 832–841

(25) Arya, G.; Panagiotopoulos, A. Z. Log-Rolling Micelles in Sheared Amphiphilic Thin Films. *Phys. Rev. Lett.* **2005**, *95*, 188301

(26) Curk, T.; Dobnikar, J.; Frenkel, D. Optimal Multivalent Targeting of Membranes with Many Distinct Receptors. *Proc. Natl. Acad. Sci. U. S. A.* **2017**, *114*, 7210–7215

(27) Debets, V. E.; Janssen, L. M. C.; Šarić, A. Characterising the Diffusion of Biological Nanoparticles on Fluid and Cross-Linked Membranes. *Soft Matter* **2020**, *16*, 10628–10639.

(28) Bochicchio, D.; Pavan, G. M. From Cooperative Self-Assembly to Water-Soluble Supramolecular Polymers Using Coarse-Grained Simulations. *ACS Nano* **2017**, *11*, 1000–1011

(29) Garzoni, M.; Cheval, N.; Fahmi, A.; Danani, A.; Pavan, G. M. Ion-Selective Controlled Assembly of Dendrimer-Based Functional Nanofibers and Their Ionic-Competitive Disassembly. *J. Am. Chem. Soc.* **2012**, *134*, 3349–3357

(30) Zhuang, J.; Garzoni, M.; Torres, D. A.; Poe, A.; Pavan, G. M.; Thayumanavan, S. Programmable Nanoassemblies from Non-Assembling Homopolymers Using Ad Hoc

Electrostatic Interactions. *Angew. Chemie - Int. Ed.* **2017**, *56*, 4145–4149

(31) Murthy Peri, M. D.; Cetinkaya, C. Spherical Nanoparticle-Substrate Adhesion Interaction Simulations Utilizing Molecular Dynamics. *J. Adhes. Sci. Technol.* **2009**, *23*, 1723–1738.

(32) Molla, M. R.; Rangadurai, P.; Pavan, G. M.; Thayumanavan, S. Experimental and Theoretical Investigations in Stimuli Responsive Dendrimer-Based Assemblies. *Nanoscale* **2015**, *7*, 3817–3837

(33) Torchi, A.; Bochicchio, D.; Pavan, G. M. How the Dynamics of a Supramolecular Polymer Determines Its Dynamic Adaptivity and Stimuli-Responsiveness: Structure-Dynamics-Property Relationships from Coarse-Grained Simulations. *J. Phys. Chem. B* **2018**, *122*, 4169–4178

(34) Bochicchio, D.; Salvalaglio, M.; Pavan, G. M. Into the Dynamics of a Supramolecular Polymer at Submolecular Resolution. *Nat. Commun.* **2017**, *8*, 147

(35) De Marco, A. L.; Bochicchio, D.; Gardin, A.; Doni, G.; Pavan, G. M. Controlling Exchange Pathways in Dynamic Supramolecular Polymers by Controlling Defects. *ChemRxiv* **2021**, DOI: https://doi.org/10.26434/chemrxiv.13655864.v2

(36) Munkhbat, O.; Garzoni, M.; Raghupathi, K. R.; Pavan, G. M.; Thayumanavan, S. Role of Aromatic Interactions in Temperature-Sensitive Amphiphilic Supramolecular Assemblies. *Langmuir* **2016**, *32*, 2874–2881

(37) Wang, F.; Klaikherd, A.; Thayumanavan, S. Temperature Sensitivity Trends and Multi-Stimuli Sensitive Behavior in Amphiphilic Oligomers. *J. Am. Chem. Soc.* **2011**, *133*, 13496–13503

(38) Fuller, J. M.; Raghupathi, K. R.; Ramireddy, R. R.; Subrahmanyam, A. V.; Yesilyurt, V.; Thayumanavan, S. Temperature-Sensitive Transitions below LCST in Amphiphilic

Dendritic Assemblies: Host-Guest Implications. *J. Am. Chem. Soc.* **2013**, *135*, 8947–8954

(39) Gao, J.; Wang, H.; Zhuang, J.; Thayumanavan, S. Tunable Enzyme Responses in Amphiphilic Nanoassemblies through Alterations in the Unimer-Aggregate Equilibrium. *Chem. Sci.* **2019**, *10*, 3018–3024

(40) Raghupathi, K. R.; Guo, J.; Munkhbat, O.; Rangadurai, P.; Thayumanavan, S. Supramolecular Disassembly of Facially Amphiphilic Dendrimer Assemblies in Response to Physical, Chemical, and Biological Stimuli. *Acc. Chem. Res.* **2014**, *47*, 2200–2211

(41) Marrink, S. J.; Risselada, H. J.; Yefimov, S.; Tieleman, D. P.; De Vries, A. H. The MARTINI Force Field: Coarse Grained Model for Biomolecular Simulations. *J. Phys. Chem. B* **2007**, *111*, 7812–7824

(42) Arnarez, C.; Uusitalo, J. J.; Masman, M. F.; Ingólfsson, H. I.; De Jong, D. H.; Melo, M. N.; Periole, X.; De Vries, A. H.; Marrink, S. J. Dry Martini, a Coarse-Grained Force Field for Lipid Membrane Simulations with Implicit Solvent. *J. Chem. Theory Comput.* **2015**, *11*, 260–275

(43) Empereur-Mot, C.; Pesce, L.; Doni, G.; Bochicchio, D.; Capelli, R.; Perego, C.; Pavan, G. M. Swarm-CG: Automatic Parametrization of Bonded Terms in MARTINI-Based Coarse-Grained Models of Simple to Complex Molecules via Fuzzy Self-Tuning Particle Swarm Optimization. *ACS Omega* **2020**, *5*, 32823–32843

(44) Bochicchio, D.; Pavan, G. M. Molecular Modelling of Supramolecular Polymers. *Adv. Phys. X* **2018**, 3, 1436408

(45) Young, P. D.; Notestein, J. M. The Role of Amine Surface Density in Carbon Dioxide Adsorption on Functionalized Mixed Oxide Surfaces. *ChemSusChem* **2011**, *4*, 1671–1678

(46) De La Llave, E.; Clarenc, R.; Schiffrin, D. J.; Williams, F. J. Organization of Alkane

Amines on a Gold Surface: Structure, Surface Dipole, and Electron Transfer. *J. Phys. Chem. C* **2014**, *118*, 468–475

(47) Ghasemi, M.; Minier, M.; Tatoulian, M.; Arefi-Khonsari, F. Determination of Amine and Aldehyde Surface Densities: Application to the Study of Aged Plasma Treated Polyethylene Films. *Langmuir* **2007**, *23*, 11554–11561

(48) Zhao, J.; Li, Y.; Guo, H.; Gao, L. Relative Surface Density and Stability of the Amines on the Biochip. *Chinese J. Anal. Chem.* **2006**, *34*, 1235–1238

(49) Marieb, E. N.; Hoehn, K. The Cardiovascular System:Blood Vessels. In *Human Anatomy & Physiology, Ninth Edition*; Pearson **2013**, pp. 712

(50) Abraham, M. J.; Murtola, T.; Schulz, R.; Páll, S.; Smith, J. C.; Hess, B.; Lindah, E. Gromacs: High Performance Molecular Simulations through Multi-Level Parallelism from Laptops to Supercomputers. *SoftwareX* **2015**, *1–2*, 19–25

(51) Berendsen, H. J. C.; van der Spoel, D.; van Drunen, R. GROMACS: A Message-Passing Parallel Molecular Dynamics Implementation. *Comput. Phys. Commun.* **1995**, *91*, 43–56

(52) Tribello, G. A.; Bonomi, M.; Branduardi, D.; Camilloni, C.; Bussi, G. PLUMED 2: New Feathers for an Old Bird. *Comput. Phys. Commun.* **2014**, *185*, 604–613

(53) Hanwell, M. D.; Curtis, D. E.; Lonie, D. C.; Vandermeerschd, T.; Zurek, E.; Hutchison, G. R. Avogadro: An Advanced Semantic Chemical Editor, Visualization, and Analysis Platform. *J. Cheminform.* **2012**, *4*, 17

(54) Wang, J.; Wolf, R. M.; Caldwell, J. W.; Kollman, P. A.; Case, D. A. Development and Testing of a General Amber Force Field. *J. Comput. Chem.* **2004**, *25*, 1157–1174

(55) Wang, J.; Wang, W.; Kollman, P. A.; Case, D. A. Automatic Atom Type and Bond Type Perception in Molecular Mechanical Calculations. *J. Mol. Graph. Model.* **2006**, *25*, 247–

260

GRAPHICAL TOC ENTRY

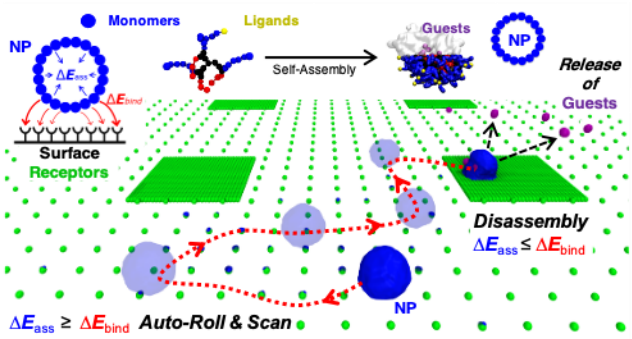

Supporting Information for:

Towards chemotactic supramolecular nanoparticles: From autonomous surface motion following specific chemical gradients to multivalency-controlled disassembly

Chiara Lionello,[†,a] Andrea Gardin,[†,a] Annalisa Cardellini,[a] Davide Bochicchio,[b,c] Manisha Shivrayan,[d] Ann Fernandez,[d] S. Thayumanavan[d] & Giovanni M. Pavan[a,b,]*

[a] Politecnico di Torino, Department of Applied Science and Technology, Corso Duca degli Abruzzi 24, Torino, 10129, Torino, Italy

giovanni.pavan@polito.it

[b] Department of Innovative Technologies, University of Applied Sciences and Arts of Southern Switzerland, Polo Universitario Lugano, Campus Est, Via la Santa 1, 6962 Lugano-Viganello, Switzerland

[c] Department of Physics, Universit_a degli studi di Genova, Via Dodecaneso 33, 16100 Genova, Italy

[d] Department of Chemistry, Center for Bioactive Delivery at the Institute for Applied Life Sciences, University of Massachusetts, Amherst, Massachusetts 01003, United States

1. Experimental Techniques

1.1. Structural Illumination Microscopy (SIM)

The quantification and rearrangement of trimeric assemblies on positively charged polylysine surfaces was carried out via Structural Illumination Microscopy (SIM). First, 1 mg of either 1, 2 or 3 COOH trimer was dissolved in 100 µL acetone. To this, a 1 mg/mL solution of DiD (1,1'-Dioctadecyl-3,3,3',3'-Tetramethylindodicarbocyanine, 4-Chlorobenzenesulfonate Salt) was loaded at 10 v/v%. 1 mL DI water was then added dropwise and stirred overnight to obtain trimeric assemblies dispersed in water and non-covalently encapsulating DiD dye. Solutions of the trimeric assemblies were then diluted to 0.05 mg/mL for SIM experiments. For experiments with SIM, a glass chamber setup was fabricated. Briefly, two pieces of clear double-sided tape of dimensions 1 cm x 3cm x 70 µm were placed on the polylysine functionalized glass slide 1 cm apart. A coverslip was then placed over the double-sided tape to form a thin chamber. For all experiments with SIM, 20 µL of the solution containing trimeric assemblies were injected into the glass chamber and the chamber washed 3X with 50 µL DI water to flush out any assemblies that were not bound to the polylysine surface. The assemblies were excited with a 640 nm laser to obtain a fluorescence signal from the encapsulated DiD and to visualize adhered assemblies on the surface. Captured images were then used to determine rearrangement of particles on the polylysine surface and for quantification.

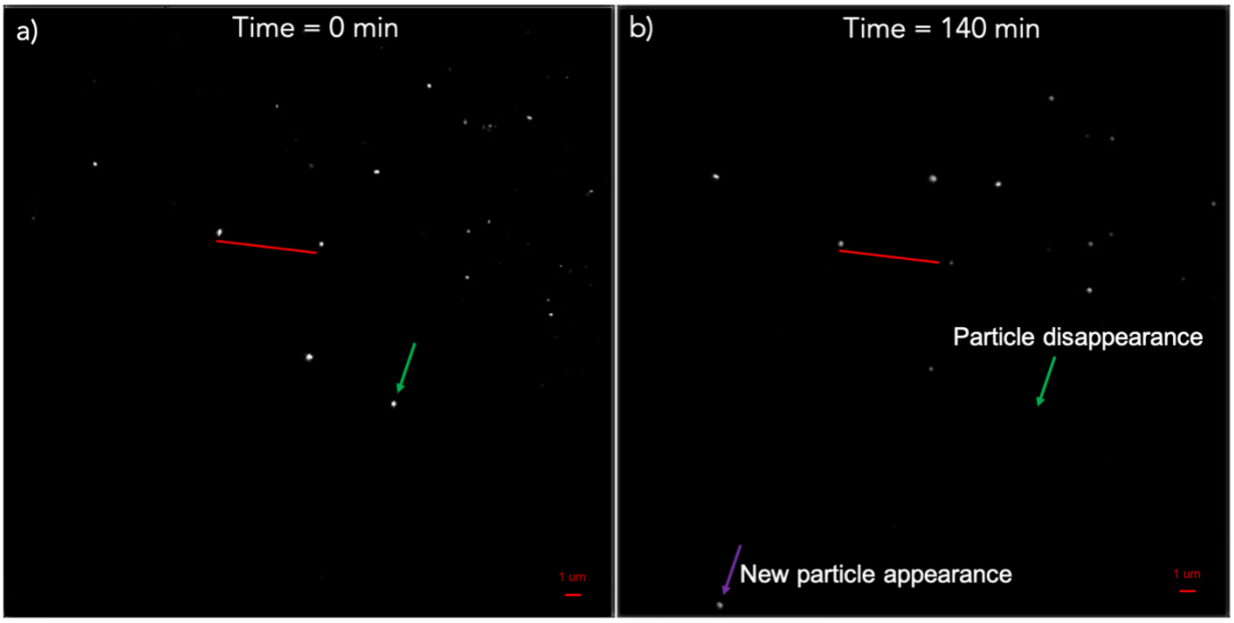

Figure S1: Structural Illumination Microscopy (SIM) images of a polylysine functionalized surface showing a) adhesion of 1-COOH trimeric assemblies at the start of the experiment and b) rearrangement of the trimeric assemblies as captured by the microscope after 140 minutes.

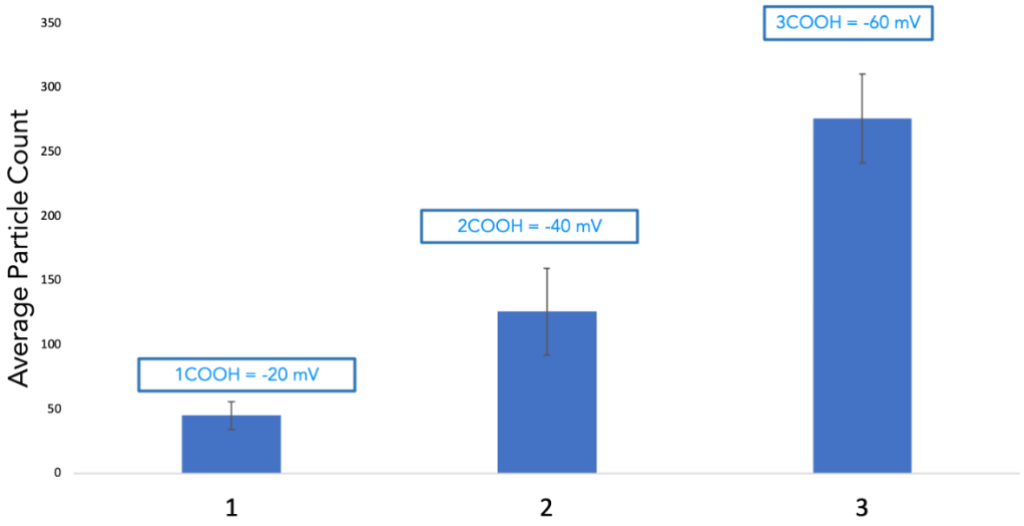

Figure S2: Quantification of trimeric assemblies on polylysine surfaces using SIM. Increasing the multivalent interaction, the average particles adhered to the surface rise up.

2. Modelling Details

2.1. Coarse-Grained (CG) Molecular Dynamics (MD) minimalistic model

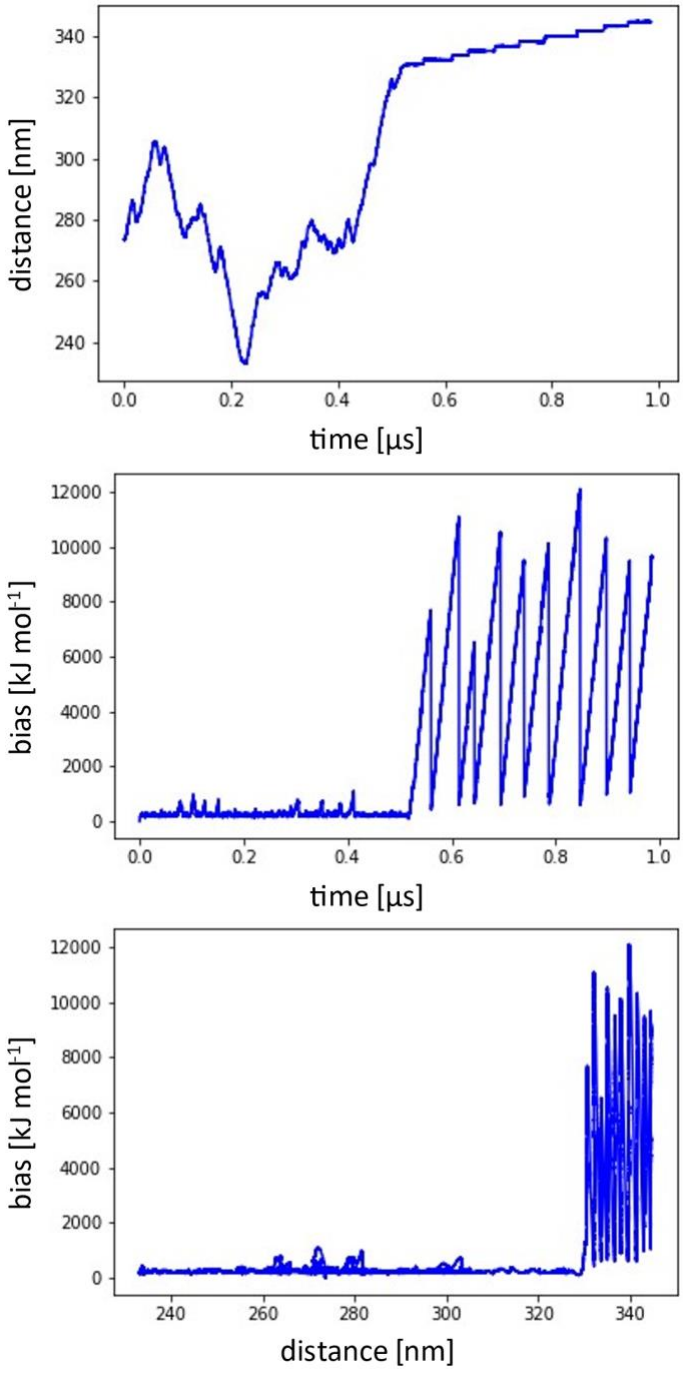

Figure S3: Metadynamics (MetaD) simulation details of the minimalistic coarse-grained (CG) supramolecular NP with encapsulated guests rolling on a receptor decorated surface. Top panel: time evolution of NP vector position. Central panel: time evolution of accumulated bias. Note that once the NP binds to the higher density surface (at time = 0.5 μs), the bias accumulated increases rapidly. Bottom panel: accumulated bias as function of NP vector position during the MetaD simulation.

2.2. Coarse-Grained (CG) Molecular Dynamics (MD) model

Well-Tempered MetaDynamics (MetaD) simulations were used to validate the dimerization Free Energy Surface (FES) profile of the Coarse-Grained (CG) model of two trimeric amphiphiles with respect to the FES profile of the all-atom (AA) model of the same dendrimer (Figure S1). Specifically, we identified two atomistic collective variables: (i) the distance between the central residues within the monomers, and (ii) the mean number of contacts between the hydrophobic residues (rational switch function and R_0 = 0.5). The CG collective variables were instead the distance between the central beads (corresponding to the central AA residue) and the mean number of contacts between the hydrophobic beads (treated in the same way as the atomistic). The two FES profiles were ultimately obtained by a reweight on the "central" distance. In both cases the simulation sofware PLUMED was used and the following simulation parameters were set: height = 2.0, biasfactor = 20, sigma = 0.05 and 0.1 for the variable distance and number of contacts respectively.

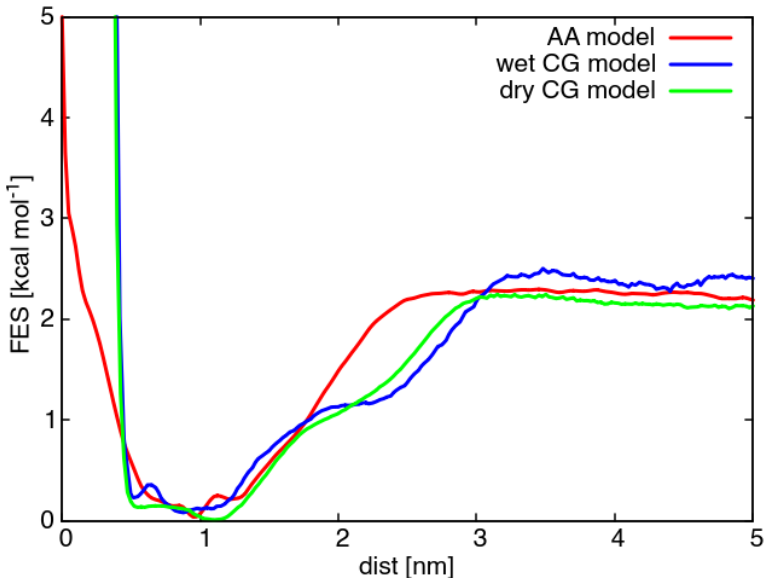

Figure S4. Free Energy Surface (FES) of trimeric amphiphile dimerization obtained with well-tempered metadynamics technique. The validation of Coarse-Grained (CG) model (blue line) has been tuned on the all-atom (AA) profile (red line) as a function of the distance between the center of the two monomers (see Figure 3a of the main paper). The distance variable refers to the COM distance (AA case) and the bead-to-bead distance (CG case) of the central residue of the standard monomer.

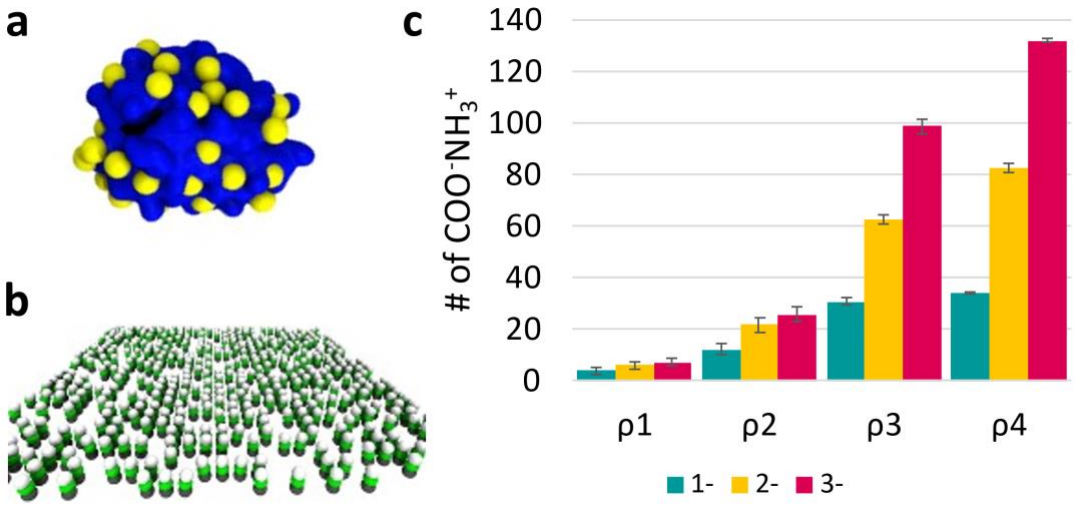

Figure S5. (a) CG-MD simulation snapshot of a single self-assembled nanoparticle made of 44 trimeric amphiphiles validated as shown in Figure S1. Color code: charged beads are depicted in yellow, while blue beads represent the complementary monomer structure. (b) An example of ligands decorated surface. The charged beads are in white, while the remaining ligands are colored in green and gray. (c) Number of contacts between the NP charged beads and the surface ligand charged beads calculated in unbiased CG-MD simulations for different ligand concentrations (ρ_1, ρ_2, ρ_3, ρ_4) and protonation states (**-1*e***, **-2*e***, **-3*e***).

2.3. Infrequent Meta Dynamics

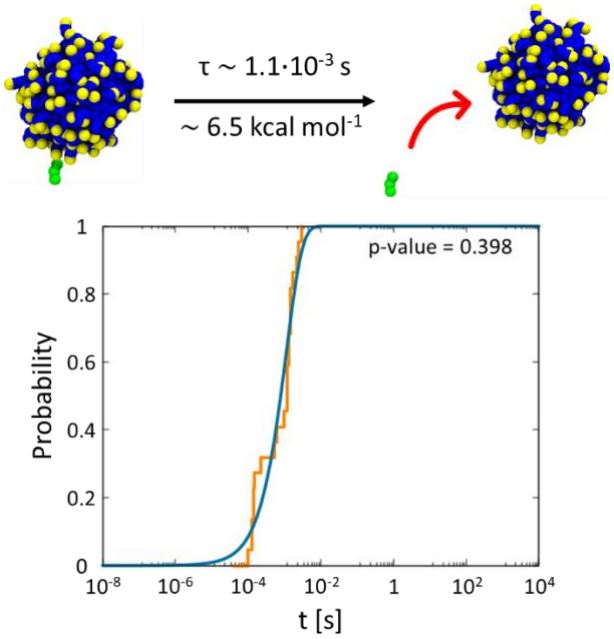

Figure S6. Transition times extracted from the infrequent MetaD simulations. The plot reports the empirical and theoretical distributions of the transition times needed to detach the **-1*e*** charged nanoparticle from a single surface ligand. We have $\boldsymbol{\tau = 1.14 \cdot 10^{-3}\ s}$ with a $\boldsymbol{p - value = 0.398}$.

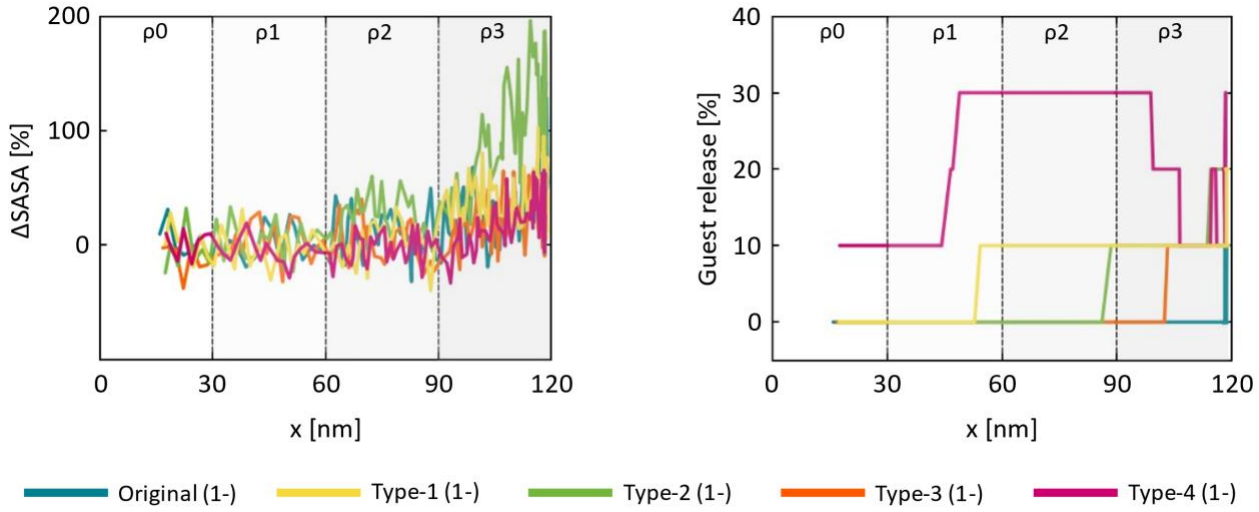

Figure S7: Comparison of ΔSASA (NP SASA variation) and percentage of guest release for NPs composed of the different trivalent (-1*e*) dendron variants. The CG models of *Original*, *Type-1*, *Type-2*, *Type-3* and *Type-4* residues are reported in Figure 6 of the main paper.

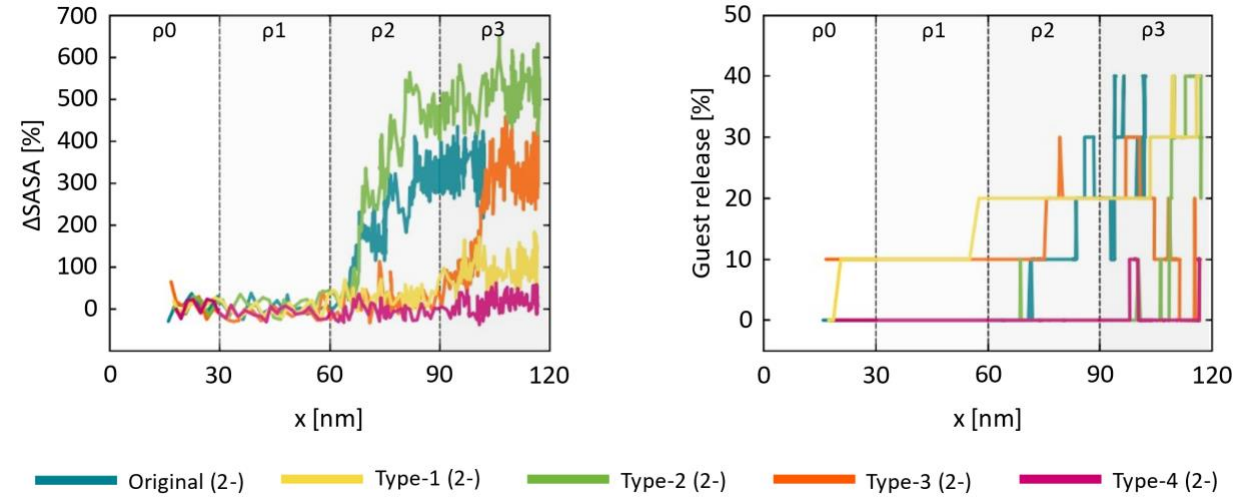

Figure S8: Comparison of ΔSASA (NP SASA variation) and percentage of guest release for NPs composed of the different trivalent (-2*e*) dendron variants. The CG models of *Original, Type-1, Type-2, Type-3* and *Type-4* residues are reported in Figure 6 of the main paper.